Journal of Volcanology and Geothermal Research 194 (2010) 55–60

Contents lists available at ScienceDirect

Journal of Volcanology and Geothermal Research

journal homepage: www.elsevier.com/locate/jvolgeores

Protocols for UV camera volcanic SO_2 measurements

Euripides P. Kantzas [a], A.J.S. McGonigle [a,b,*], Giancarlo Tamburello [c], Alessandro Aiuppa [b,c], Robert G. Bryant [a]

[a] Department of Geography, University of Sheffield, Winter Street, Sheffield, S10 2TN, UK
[b] INGV, Sezione di Palermo, Via Ugo La Malfa 153, Palermo, Italy
[c] Dipartimento CFTA, Via Archirafi 36, 90123, Università di Palermo, Palermo, Italy

ARTICLE INFO

Article history:
Received 6 January 2010
Accepted 3 May 2010
Available online 8 May 2010

Keywords:
ultraviolet camera
volcanic SO_2 monitoring
volcanic gas geochemistry

ABSTRACT

Ultraviolet camera technology offers considerable promise for enabling 1 Hz timescale acquisitions of volcanic degassing phenomena, providing two orders of magnitude improvements on sampling frequencies from conventionally applied scanning spectrometer systems. This could, for instance enable unprecedented insights into rapid processes, such as strombolian explosions, and non-aliased corroboration with volcano geophysical data. The uptake of this technology has involved disparate methodological approaches, hitherto. As a means of expediting the further proliferation of such systems, we here study these diverse protocols, with the aim of suggesting those we consider optimal. In particular we cover: choice and set up of hardware, calibration for vignetting and for absolute concentrations using quartz SO_2 cells, the retrieval algorithm and whether one or two filters, or indeed cameras, are necessary. This work also involves direct intercomparisons with narrowband observations obtained with a scanning spectrometer system, employing a differential optical absorption spectroscopic evaluation routine, as a means of methodological validation.

1. Introduction

Recently, ultraviolet (UV) cameras have been developed for imaging SO_2 emissions in a volcanological context (Mori and Burton, 2006; Bluth et al., 2007). This technique provides many advantages: such as ready spatial alignment with the emissions from a static observational point and data capture with a temporal resolution of order 1 Hz. Further, the camera images are used to directly calculate the plume transport velocity, via cross correlation methods (e.g., McGonigle et al., 2005; Williams-Jones et al., 2006), significantly reducing the magnitude of this source of error, which has been a blight upon previous SO_2 flux assessments.

This technology heralds the much awaited prospect of capturing transient (≤tens of seconds) volcanic degassing driven phenomena, with UV remote sensing, such as Strombolian (Mori and Burton, 2009) and Vulcanian (Yamamoto et al., 2008) explosions, which are too fast to be resolved using conventional scanning spectroscopic (few minute sampling) means (e.g., Edmonds et al., 2003; McGonigle et al., 2003). Furthermore, the possibility of non-aliased corroboration between volcanic degassing and geophysical (≈1 Hz) data streams, as recently achieved with a related approach by McGonigle et al. (2009), offers promise to significantly deepen our volcanological understanding. Earlier attempts at such multi-parametric analyses, albeit on the basis of the then available far coarser time resolution SO_2 fluxes, have confirmed the great potential contained therein (e.g., Fischer et al., 1994; Watson et al., 2000).

To date the uptake of this technology has involved a number of research groups pursuing distinct operating methodologies. In order to expedite the widest scale dissemination of this technology, so facilitating the enormous potential contained therein, we extensively investigate such protocols here, presenting conclusions on those which we consider to be optimal for this application. This work was performed during a field campaign on Mt Etna from July 12–19 2009.

2. Hardware

In these experiments we used two Apogee Instruments Alta U260 cameras, each fitted with a 16 bit 512×512 pixel Kodak KAF-0261E CCD detector. These units provided more than enough spatial resolution in all our observations, ranging <0.5–20 km from Mount Etna's plume, and also during related studies on Vulcano and Stromboli. Furthermore, readout times were considerably reduced, offering scope for faster acquisition frequencies, relative to alternate 1024×1024 pixel detector cameras. In most cases, for an equivalent camera field of view, the 512 pixel array provides greater signal to noise, by virtue of the factor of four larger sky area imaged per pixel. The one possible exception to this is the Alta U47, equipped with broadband coating, which at almost twice the price of the U260 (≈$13,000 vs. ≈$7000) does have a factor of ≈2.75 more sensitive detector at 400 nm. Whilst comparative data for the spectral region of interest (≈300–340 nm) are unavailable, this unit could feasibly be more than four times more UV sensitive in this window.

These detectors were thermo-electrically cooled to ≈30 °C below ambient temperature, with each camera consuming up to 40 W, from a 12 V battery power supply. The units were mounted on a steel rail,

* Corresponding author. Department of Geography, University of Sheffield, Winter Street, Sheffield, S10 2TN, UK. Tel.: +44 0 114 222 7961; fax: +44 0 114 279 7900.
E-mail address: a.mcgonigle@shef.ac.uk (A.J.S. McGonigle).

0377-0273/$ – see front matter © 2010 Elsevier B.V. All rights reserved.
doi:10.1016/j.jvolgeores.2010.05.003

Fig. 1. Cameras imaging SO_2 emissions ≈2 km from the summit craters of Mt. Etna. The telescopes between the cameras were incidental to the camera set up.

atop a tripod, and co-aligned to ensure identical pointing configurations, as shown in Fig. 1. Data capture and processing were achieved with custom written LabVIEW code, from a single laptop computer, with typical sampling rates ≈0.5 Hz, and single image sizes ≈0.5 Mb for 16 bit png format. Far faster acquisitions (≈10 Hz) could be achieved, however by using the camera's internal memory, or by reducing the radiometric or spatial resolution.

Each camera was coupled to a Pentax B2528-UV lens of $f=25$ mm focal length, providing a full angle field of view (FOV) ≈24°. The FOV must be set to permit total capture of the plume cross section from the desired measurement location, whilst ensuring that the profile is composed of a reasonable number of pixels. Coupled with this is the requirement, where safely possible, to minimise the plume-instrument distance. This reduces errors associated with scattering of light from outside the plume into the sensor FOV, and dispersal of radiation, targeted at the sensor within the plume, yet scattered away from the FOV, subsequently (e.g., Mori et al., 2006; Bluth et al., 2007; Kern et al., 2009). This can be achieved, for instance, by laterally observing the horizontally advecting plume, at a distance from the source, but in relative proximity to the gases, rather than imaging the plume rising above the crater, nearer to the summit. The rather wide FOV, from our short f lens, expedited imaging the entire plume cross section, from closer vantage points than possible with longer f commercially available alternates.

Immediately in front of each lens, a 10 nm full width at half maximum (FWHM) bandpass filter was placed in an in house built mount, which also accommodated the quartz SO_2 cells used in the calibration. These filters were centred on 310 nm (Asahi Spectra XBPA310; affected by plume SO_2 absorption) and 330 nm (XBPA330; where SO_2 doesn't absorb), respectively. A key factor in these measurements is the inhomogeneous illumination of the detector across the field of view, causing darkening towards the image extremes, which must be addressed somehow. This is caused by vignetting: a fundamental property of the lens-aperture system, and the filters' transmissions, whose peaks shift to shorter wavelengths, where skylight illumination is reduced, with increasing incident angle.

Vignetting is exacerbated by widening the lens aperture. However, given that, in practice, it is extremely simple to characterise, to accommodate for this, and the signal to noise benefits of widening the iris, for all pixels across the image, so enabling higher sampling frequency acquisitions, we set the aperture to the maximum F2.8, F-number setting throughout. Furthermore, at smaller iris dilations, we noted triangular aberrations in the image arising from the aperture geometry, which could severely compromise the SO_2 retrieval (e.g., as shown in Fig. 2).

3. Calibration

The first element to the calibration involves characterising the instrumental vignetting. This is necessary for most, but not all, measurement configurations, as shall be detailed in the following section. Whilst the vignetting can be ascertained from images containing the volcanic plume, it is better to avoid this perturbing influence upon some of the pixels, to provide the most data points for the analysis. The simplest way to do this is to point the camera away from the sun at a cloudless sky, at 45° zenith angle at around 10:00 or 16:00 when the sun is neither at zenith nor the horizon so the imaged sky is uniformly illuminated. Images should be collected according to

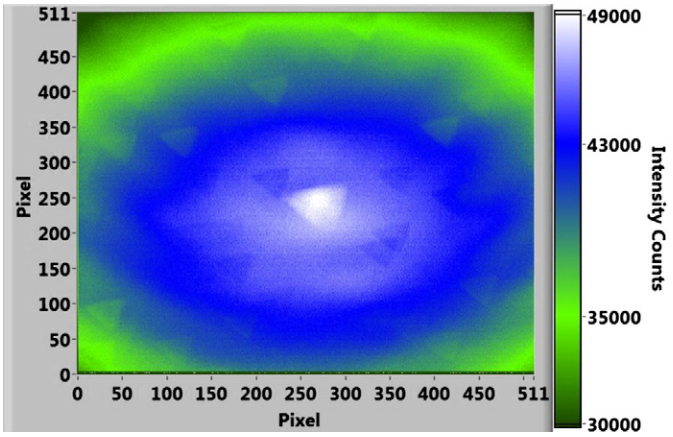

Fig. 2. A typical clear sky image from one of the cameras, with the minimum lens aperture setting, revealing the resulting triangular aberrations, which disappeared entirely when the iris was fully opened.

the approximate digital number (DN) values of the plume acquisitions themselves, given the slight nonlinearity in the camera response e.g., this would normally correspond to near saturating the 330 nm filter, and around 10% of the maximum counts for the 310 nm case. Once one image is collected per filter, this is normalised with respect to its maximum pixel intensity to create a mask, which all subsequently acquired images are divided by, to correct for vignetting.

The camera technique operates on the principle of contrasting the brightness of the pixels in the presence/absence of SO_2 absorption. This can be done with two filters (e.g., at 310 and 330 nm, where UV radiation is/is not absorbed, respectively), in which case a qualitative measure of absorbance A is measured per camera pixel:

$$A = -\log_{10}\left[(IP_{310} / IB_{310}) / (IP_{330} / IB_{330})\right] \quad (1)$$

In this case IP and IB are the dark image subtracted, then vignette corrected, plume and background sky images, taken with either the 310 or 330 nm filter installed, as specified by the subscript. This can be achieved with two cameras, one with each filter, or with a single camera in which case the filters are alternately placed over the lens. Dark image collection, by covering the camera lens, is necessary to accommodate for dark current and electronic offset. As these phenomena are quasi-constant, over timescales of 1 hour, following the ten minute switch on thermal stabilisation, a single dark image, per camera, will suffice for such an acquisition duration. The alternate is to use a single filter in a spectral region where SO_2 is absorbed (e.g., 310 nm), in which case A is measured as:

$$A = -\log_{10}\left[IP_{310} / IB_{310}\right] \quad (2)$$

These qualitative measures of concentrations are then calibrated via placing a series of quartz calibration cells, containing known SO_2 column amounts in front of the filter(s). For consistency, we used cells of equal diameter (25 mm; Resonance Ltd.) to the filters, placed immediately in front of the filters in the in house built mounts. The SO_2 concentration per cell is then plotted against A (in our case averaged over the central 200×200 pixel section), measured as above, and the line's gradient taken as the calibration ratio. The latter is then multiplied by subsequently acquired plume images' pixel A values to convert them to ppm m. Four or more cells of well spaced concentrations should be used to obtain a reliable linear fit, up to around 1800 ppm m, where the absorption saturates. Our cell column amounts were: 100, 212, 400, 1060 and 1540 ppm m.

Using the two cameras, each equipped with one filter, we validated that the cell calibration ratios per pixel were constant across the central 200×200 section of the image, ruling out any error source arising from the wavelength dependent filter transmission characteristics in this region. Due to spurious reflections from the cell side walls we could not extend this study to the pixels closer to the image edges. This merits further attention, perhaps using wider cells to determine whether, for instance, different calibration ratios need to be applied for the more peripheral pixels. We further confirmed that the calibration ratios are also unaffected by heating/cooling the filters by 15 ° C with respect to room temperatures (≈18 °C).

We have adopted the approach of employing the same integration time for acquisitions with both filters. This corresponds to near saturating the 330 nm image (to maximise signal to noise), where background skylight illumination is far more intense than at 310 nm, providing the highest possible time resolution, taking full advantage of the cameras' rapid acquisition capability. This further maximises the plume spatial coherence between the different filter images. Dalton et al. (2009) note a variation in calibration ratio for exposure times set at the same per filter, or where they are independently determined so to near saturate the cameras at 310 and 330 nm (the former filter typically permits transmission of around 15% the intensity from the latter). In and of itself this issue is unimportant, so long as calibration is performed under the acquisition and illumination conditions of the measurement itself. The key issue is whether the data best fit line, from which, the gradient e.g., ratio is derived, has sufficient goodness of fit.

In order to investigate this further, we performed cell calibrations with the 330 nm filter near saturated, and the 310 nm filter view exposed to provide peak pixel intensities ranging between ≈10 and 90% of the maximum DN. These calibration ratios, obtained by averaging pixel intensities per cell measurement, over the central 200×200 array subset, varied by only 6% between end members. Most importantly, however the fit line R^2 was ≥0.999 in all cases. Hence, so long as calibration is made under the same conditions as the measurements themselves, so that the appropriate ratio is used, there is no advantage here to near saturation of the 310 nm filter acquisitions. The only possible caveat to this, which may in part explain the disparity between our results, and the rather lower R^2 values reported by Dalton et al. (2009), relates to circumstances where illumination is poor, such that the 310 nm:330 nm intensity ratio is considerably lower than encountered in our measurements. Under such circumstances it may be necessary to increase the 310 nm exposure to obtain good calibration line R^2 fitting. We found that calibrations were valid for periods of an hour or so where illumination conditions were constant, however for variable cloud cover and near sunrise and sunset more regular calibration may be necessary.

4. Measurement

The measurement involves capturing the plume and background sky images, so to compute the qualitative measure of plume absorbance, A, per pixel, as described above. Ideally the plume-camera-sun angle should be at least 90° to avoid issues associated with strongly inhomogeneous illumination across the field of view and for the flux computation, clear sky should be contained in the image either side of the plume. Meteorological cloud behind the camera field of view does not appear to be overly problematic, however clear/uniformly cloudy sky backgrounds are optimal. Cloud between the observer and plume, however will likely render measurement impossible.

The retrieval can be accomplished in a number of different ways. Firstly, where there is clear sky adjacent to the plume view, this can be used as a proxy for background illumination (e.g., Mori and Burton, 2006). In this case, vignetting does not need to be considered as this effect is cancelled out when the plume/background sky image ratios are computed. Once A values are calculated for each pixel, the baseline A value, for those parts of the image containing no SO_2 is subtracted, then ppm m values generated, with multiplication by the calibration ratio. In principle, this could be the most accurate possible retrieval methodology, however it can be frustrated where the volcano or sun obstructs capture of a near plume background image.

We have also worked with two further approaches, where, for simplicity, no background image collection is required, and the background skylight characterised, rather from portions of clear sky viewed in the plume image. At least 75 pixels of clear sky should ideally be present in both sides of any row/column of interest for them to work, and vignette correction is required. In the first such case, the second method, the intensity across such lines is plotted and the variation in background illumination across the image characterised with a polynomial fit (1st or 2nd degree is adequate) to those pixels not within the plume. These polynomial coefficients are then used for each column/row to generate modelled background images, from which A, and ppm m, values are derived according to the first method.

Finally, we also used a third method, which is a simplification of the second, yet demands less user intervention hence has better scope for fully autonomous retrievals. This is based on rearranging Eq. (1) into the components:

$$A = -\log_{10}(IP_{310} / IP_{330}) - \log_{10}(IB_{330} / IB_{310}) \quad (3)$$

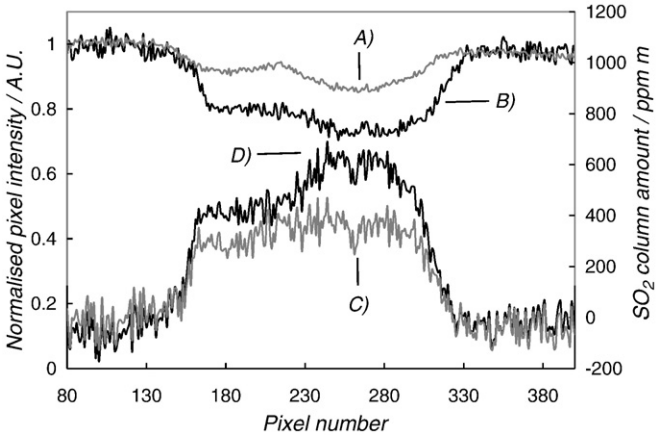

Fig. 3. Example vignette corrected normalised pixel intensities across the plume profile for both 330 nm and 310 nm views [A) and B) respectively; plotted against the primary axis]. The resulting SO_2 column amounts are shown [C); secondary axis], as derived from method 3, based on the measurement with both filters. For comparison, concentrations based on observations of the 310 nm attenuation alone are also presented [D); secondary axis]. Such strong disparities, which we frequently observed between these two column amount profiles, issue a caution against indiscriminate single filter operation.

We found that it is a good approximation to assume that $\log_{10}(IB_{330}/IB_{310})$ is constant across the image, even where clouds are present behind the plume, e.g., Eq. (3) is recast as:

$$A = -\log_{10}(IP_{310}/IP_{330}) + constant \quad (4)$$

This approach relies, therefore on simply taking the logarithm of the ratio of the two vignette corrected, dark subtracted filter images of the plume. A scalar is then subtracted from the resulting image to deal with the constant term in Eq. (4) by automatically finding the baseline value, and then the calibration ratio is used to convert to ppm m. Fig. 3 shows intensities of lines, through the plume, from example contemporaneous 310 nm and 330 nm plume views, and the resulting ppm m concentration profile, determined via method 3.

Fig. 4 shows an example of cross plume concentration profiles, obtained at around 1 km from Mt Etna's craters, using the above three methods, illustrating the excellent agreement between the three; the associated plume concentration image is shown in addition. On the basis of simplicity and the fact it is apparently unnecessary to capture a background image, we have used method 3 routinely, leading to the results detailed below. However as a quality control check, where possible we periodically collected a background image, and enacted method 1 in parallel. Once image concentrations are calculated, they are integrated with respect to distance over the plume cross section, to generate so called integrated column amounts (ICAs) for the pixel row or column of interest. By cross correlating time series from two such parallel and spatially segregated ICA series, the plume speed is generated, which, when multiplied by one such ICA series, outputs fluxes.

As a means of further quantitative testing, we compared our camera observations with those from a scanning spectrometer system, of 1.8° step, as detailed in McGonigle et al. (2003), and containing an Ocean Optics USB2000+ (Kantzas et al., 2009). The spectral data were processed using the UVolc code, a development of volcanoSO2.exe (McGonigle, 2007) which provides better spectral fitting and wavelength and linewidth alignment. The optical axes of the scanner and cameras were affixed at right angles to a machined bar, so to scan through profiles of the horizontally advecting plume, corresponding to the central pixel column of the camera FOV at locations 1 km and 12 km from the gas. In all cases the plume was viewed approximately orthogonally to its propagation vector. Some thirty such profile intercomparisons were performed, demonstrating broad agreement (typically within ≈15%) in all cases, such as in the sample plots shown in

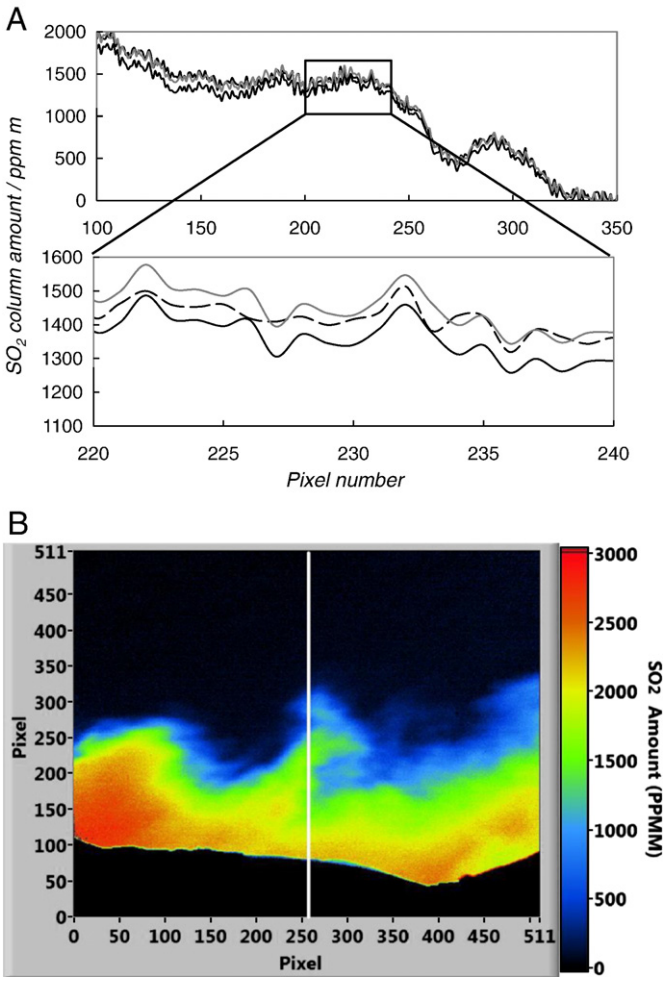

Fig. 4. A) Intercompared plume profile SO_2 concentrations calculated using retrieval methods 1 (dashed black line), 2 (black line) and 3 (grey line). The whole profile is shown at top, and a zoomed sub section, for clarity, beneath. There is good agreement between all three traces, with the outputs of methods of 1 and 3 overlapping particularly strongly; B) shows the corresponding plume concentration image (method 3), from which A) portrays data concerning column 256 (denoted in the image with the vertical white line). Note that in A) the ground pixels to the left of the plots, where the retrievals are invalid, and the extended zero concentration baselines to the right have been omitted for clarity. Whilst the highest concentrations shown here are likely to involve absorption saturation, leading to systematic errors, this will apply equally to all three methods; the intercomparison is not compromised as a consequence, therefore.

Fig. 5. This provides confidence in the inter calibration of both approaches, hence the scope of the UV camera to succeed spectrometer based SO_2 flux observations (e.g., McGonigle et al., 2002; Galle et al., 2003), under appropriate circumstances. Further work now remains in advancing the efforts of Kern et al. (2009) in considering the exact under or overestimations incurred in both the spectroscopic and camera based SO_2 retrievals, caused by in-plume and between plume and observer UV scattering. Future lines of enquiry could involve characterising these errors using spectroscopic data then using this information to correct parallel UV camera concentrations.

As part of this exercise we also compared mean scanner concentrations across the plume profile, measured 12 km away, against those from a USB2000+, coupled to a telescope of rectangular, vertically oriented, FOV (≈0.3°×14°), spatially filtered to match the ≈12° vertical width plume. Pairs of the latter have been applied to generate integrated column amounts, with multiplication of the outputted concentrations, taken as proxies for the mean column amount across the field of view, by the field of view length at the plume distance. Such data have been used to generate high time resolution SO_2 fluxes, by analogy to the camera methodology (McGonigle et al., 2009; Boichu

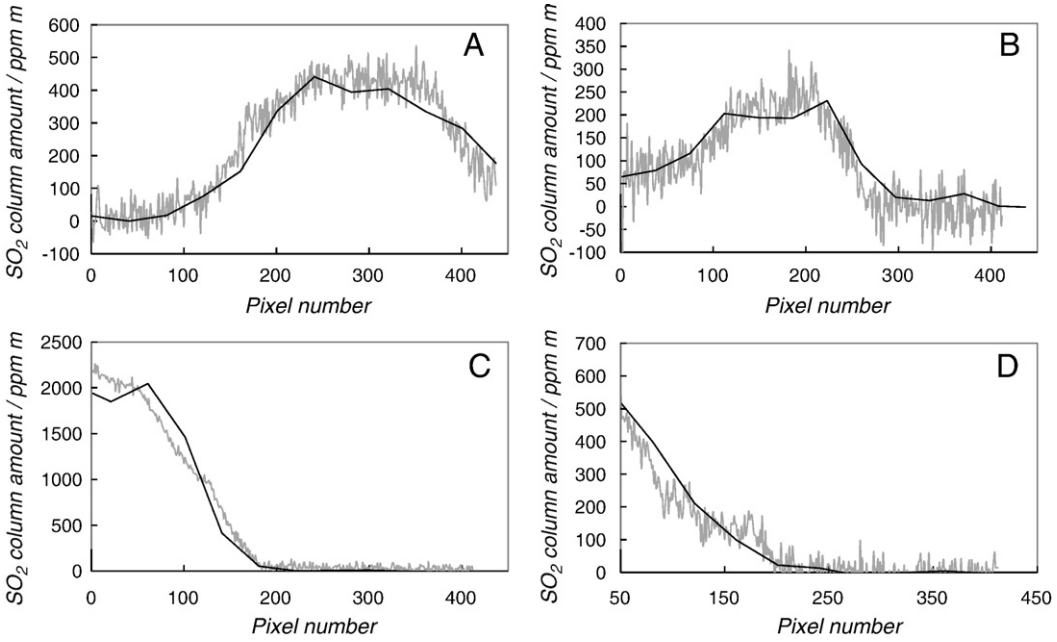

Fig. 5. Example retrieved plume concentration profiles from the UV cameras (in grey) compared against those from a scanning spectrometer (in black). Each angular concentration datum from the latter is projected onto the corresponding camera pixel value, demonstrating broad methodological agreement in all cases. Data were captured at ≈12 km from the gas [A) and B)], and ≈1 km away [C) and D)], respectively. The plume was at low elevation for plots C) and D), such that the whole cross section could not be captured. Whilst saturation will affect the highest retrieved concentrations in C), this effect should apply to the spectrometer and camera observations in a broadly similar fashion, therefore perturbing the absolute retrieved concentrations, but not the integrity of the intercomparison.

et al., 2010). In our experiments, good correspondence was found between the mean scanner concentrations and those from the rectangular field of view instrument, e.g., as shown in Fig. 6. This supplies further confidence in this methodology, as a cheaper alternate to the cameras, albeit involving more complex alignment, for obtaining high time resolution SO_2 fluxes, for users already in possession of two USB2000/2000+ spectrometers.

Whilst our UV camera work was performed using two filters, other workers have used one, with the benefit of providing a simpler measurement configuration. The difficulty with a single filter, however is that one is measuring the plume attenuation caused by the gas and aerosol mixture, with no means of discriminating between the two. With two filters, the 330 nm image captures the perturbation to incident UV radiation caused by the aerosols, outside the SO_2 absorption window. The retrieval then assumes this to apply equally to the 310 nm image, where SO_2 does absorb, so that the attenuation caused by the SO_2 can be isolated. During our Etna fieldwork we investigated the effect of omitting the second filter for all of our ≈100 dataset acquisitions,

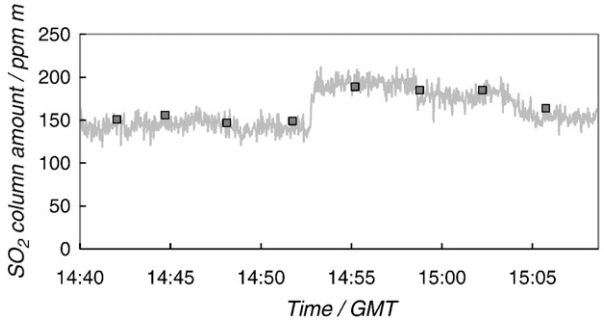

Fig. 6. Time series average concentrations across the plume profile for scanning spectroscopic observations (square points), versus SO_2 columns from a rectangular field of view spectrometer (higher time resolution grey data series) set to match the plume width. The observed agreement provides additional confidence in the latter approach as an alternate to the UV cameras for acquisition of high time resolution SO_2 fluxes, albeit demanding more complex alignment.

finding that this could lead to both strong both strong over and underestimations to SO_2 concentrations, with additional absorption in the former case and backscatter in the latter. Furthermore, during preliminary power station measurements, where the SO_2 plume was rather condensed, we found the plume pixels at 310 nm to be brighter than the background sky, which would result in negative retrieved concentrations. This effect is very situational and can vary across the plume, depending upon the degree of condensation as well as the location of the sun in the sky.

Fig. 3 shows a sample plume cross section for both 310 nm and 330 nm filters, indicating the clear plume aerosol attenuation at 330 nm. Resulting concentration profiles from method 3 using both filters are shown alongside an analogous treatment based on the 310 nm filter alone. In the latter case IB_{310} in Eq. (2) for each in-plume pixel is taken as the value of IP_{310} found immediately outside the plume. It is clear in this case that the aerosol effect causes significant overestimation (≈50%) of the SO_2 column. We therefore strongly counsel the use of two filters, even if the 330 nm one is only used periodically, to gain a rough sense of imposed systematic error.

Where two filters are used, one has the option of using a single camera, and changing the filters manually or automatically, or using two cameras as we have done, with a filter dedicated to each, albeit at greater cost. The fundamental issue here is how much the plume structure changes between acquisitions with the 310 nm and 330 nm filters. Allowing for a second to switch between acquisitions, so long as identical acquisitions times are used for each filter, we found that the retrieval was not adversely affected for observations at distances of >1 km from source and typical plume transport speeds (5–10 m s^{-1}). However closer to source intolerable spatial incoherence was introduced via the shorter time taken for the plume to transit the camera's field of view. In principle this can perhaps be compensated for by linearly shifting one filter plume profile, to overlap that of the other; however as the plume profile also evolves temporally, this could be extremely difficult in practice. For this reason, it was necessary to use two cameras under such circumstances to provide total spatial and temporal coherence between filter views. This would be particularly valuable in monitoring very transient degassing phenomena, such as

strombolian explosions, of timescales of tens of seconds, where gases propagate at high speeds.

5. Summary

Here we have investigated distinct methodological possibilities in measuring SO_2 emissions with ultraviolet cameras. This technology is likely to be of increasing value in observational volcanology in the coming years, in particular in providing volcano gas geochemical data which mimic geophysical observations in respect of time resolution. Our key empirical suggestions are that: 1. operation with two filters is extremely important, if only to use the 330 nm filter periodically to gain a sense of systematic error associated with aerosol attenuation/backscatter; two cameras enable dual filter views of rapid degassing phenomena; 2. concentration retrievals do not appear to demand capture of a background plume image; 3. there is no advantage to having longer exposure times for the 310 nm filter than for 330 nm, unless specifically identified low light circumstances demand them; 4. operation with the lens aperture fully open improves signal to noise; whilst this enhances vignetting, the latter can be straightforwardly accounted for; 5. we found that 512×512 array cameras provided sufficient spatial resolution for these measurements with the benefit of reduced readout times; further our relatively short *f* lens expedited capturing the plume cross section from closer vantage points than possible with longer lenses, mitigating against scattering related errors. These instrumental factors need to be individually considered for each volcano, however, depending on the available monitoring locations, and the imperative to remain at safe distances from the summit; 6. the cell calibration ratio was consistent across the central image section, however further work is required on determining whether this might vary more peripherally.

This study also revealed heartening correspondence between scanning spectrometer and UV camera plume cross sectional concentrations under a variety of circumstances, validating the technological transition from the former to the latter approaches where desired. Whilst the UV camera carries many advantages, in respect of its simplicity, this broadband spectral output has limited scope for managing errors associated with aerosol scattering. To this end, a key future objective would be to operate cameras and spectrometers in parallel, and employ the more sophisticated retrievals, concerning the latter, detailed in Kern et al. (2009), to characterise and so compensate for this uncertainty source in the camera data.

Acknowledgements

We acknowledge with gratitude those who have supported this work: in particular Sergio Gurrieri, Marco Liuzzo and Gaetano Giudice of INGV Palermo and RCUK for an Academic Fellowship to AMcG. We thank Toshiya Mori, Felix Kick and Christoph Kern for their very helpful advice. Finally we thank Giovanni Chiodini for his editorship, Marika Dalton and another (anonymous) reviewer for their much appreciated investment of time in appraising this paper.

References

Bluth, G.J.S., Shannon, J.M., Watson, I.M., Prata, A.J., Realmuto, V.J., 2007. Development of an ultra-violet digital camera for volcanic SO_2 imaging. J. Volcanol. Geotherm. Res. 161, 47–56. doi:10.1016/j.jvolgeores.2006.11.004.

Boichu, M., Oppenheimer, C., Tsanev, V., Kyle, P.R., 2010. High temporal resolution SO_2 flux measurements at Erebus volcano. Antarctica. J. Volcanol. Geotherm. Res. 190, 325–336. doi:10.1026/j.jvolgeores.2009.11.020.

Dalton, M.P., Watson, I.M., Nadeau, P.A., Werner, C., Morrow, W., Shannon, J.M., 2009. Assessment of the UV camera sulfur dioxide retrieval for point source plumes. J. Volcanol. Geotherm. Res. 188, 358–366. doi:10.1016/j.jvolgeores.2009.09.013.

Edmonds, M., Herd, R.A., Galle, B., Oppenheimer, C.M., 2003. Automated, high time-resolution measurements of SO_2 flux at Soufrière Hills Volcano. Montserrat. Bull. Volcanol. 65, 578–586. doi:10.1007/s00445-003-0286-x.

Fischer, T.P., Morrissey, M.M., Calvache, M.L., Gomez, D., Torres, R., Stix, J., Williams, S.N., 1994. Correlations between SO_2 flux and long-period seismicity at Galeras Volcano. Nature 368, 135–137. doi:10.1038/368135a0.

Galle, B., Oppenheimer, C., Geyer, A., McGonigle, A.J.S., Edmonds, M., Horrocks, L.A., 2003. A miniaturised ultraviolet spectrometer for remote sensing of SO_2 fluxes: a new tool for volcano surveillance. J. Volcanol. Geotherm. Res. 119, 241–254. doi:10.1016/S0377-0273(02)00356-6.

Kantzas, E.P., McGonigle, A.J.S., Bryant, R.G., 2009. Comparison of low cost miniature spectrometers for volcanic SO_2 emission measurements. Sensors 9, 3256–3268. doi:10.3390/s90503256.

Kern, C., Deutschmann, T., Vogel, L., Wöhrbach, M., Wagner, T., Platt, U., 2009. Radiative transfer corrections for accurate spectroscopic measurements of volcanic gas emissions. Bull. Volcanol. 72, 233–247. doi:10.1007/s00445-009-0313-7.

McGonigle, A.J.S., 2007. Measurement of volcanic SO_2 fluxes with differential optical absorption spectroscopy. J. Volcanol. Geotherm. Res. 162, 111–122. doi:10.1016/j.jvolgeores.2007.02.001.

McGonigle, A.J.S., Oppenheimer, C., Galle, B., Mather, T.A., Pyle, D.M., 2002. Walking traverse and scanning DOAS measurements of volcanic gas emission rates. Geophys. Res. Lett. 29, 1985. doi:10.1029/2002GL015827.

McGonigle, A.J.S., Oppenheimer, C., Hayes, A.R., Galle, B., Edmonds, M., Caltabiano, T., Salerno, G., Burton, M., Mather, T.A., 2003. Sulphur dioxide fluxes from Mount Etna, Vulcano and Stromboli measured with an automated scanning ultraviolet spectrometer. J. Geophys. Res. 108 (B9), 2455. doi:10.1029/2002JB002261.

McGonigle, A.J.S., Hilton, D.R., Fischer, T.P., Oppenheimer, C., 2005. Plume velocity determination for volcanic SO_2 flux measurements. Geophys. Res. Lett. 32, L11302. doi:10.1029/2005GL022470.

McGonigle, A.J.S., Aiuppa, A., Ripepe, M., Kantzas, E.P., Tamburello, G., 2009. Spectroscopic capture of 1 Hz volcanic SO_2 fluxes and integration with volcano geophysical data. Geophys. Res. Lett. 36, L21309. doi:10.1029/2009GL040494.

Mori, T., Burton, M., 2006. The SO_2 camera: a simple, fast and cheap method for groundbased imaging of SO_2 in volcanic plumes. Geophys. Res. Lett. 33, L24804. doi:10.1029/2006GL027916.

Mori, T., Burton, M., 2009. Quantification of the gas mass emitted during single explosions on Stromboli with the SO_2 imaging camera. J. Volcanol. Geotherm. Res. 188, 395–400. doi:10.1016/j.jvolgeores.2009.10.005.

Mori, T., Mori, T., Kazahaya, K., Ohwada, J., Hirabayashi, J., Yoshikawa, S., 2006. Effect of UV scattering on SO_2 emission rate measurements. Geophys. Res. Lett. 33, L17315. doi:10.1029/2006GL026285.

Watson, I.M., Oppenheimer, C., Voight, B., Francis, P.W., Clarke, A., Stix, J., Miller, A., Pyle, D.M., Burton, M.R., Young, S.R., Norton, G., Loughlin, S., Darroux, B., Staff, M.V.O., 2000. The relationship between degassing and deformation at Soufriere Hills volcano. Montserrat. J. Volcanol. Geotherm. Res. 98, 117–126.

Williams-Jones, G., Horton, K.A., Elias, T., Garbeil, H., Mouginis-Mark, P.J., Sutton, A.J., Harris, A.J.L., 2006. Accurately measuring volcanic plume velocity with multiple UV spectrometers. Bull. Volcanol. 68, 328–332. doi:10.1007/s00445-005-0013-x.

Yamamoto, H., Watson, I.M., Phillips, J.C., Bluth, G.J., 2008. Rise dynamics and relative ash distribution in vulcanian eruption plumes at Santiaguito Volcano, Guatemala, revealed using an ultraviolet imaging camera. Geophys. Res. Lett. 35, L08314. doi:10.1029/2007GL032008.